11th World Congress on Computational Mechanics (WCCM XI)
5th European Conference on Computational Mechanics (ECCM V)
6th European Conference on Computational Fluid Dynamics (ECFD VI)
E. Oñate, J. Oliver and A. Huerta (Eds)

SHEAR WAVE PROPAGATION MODELING IN MAGNETIC RESONANCE ELASTOGRAPHY USING THE LOCAL INTERACTION SIMULATION APPROACH

Z. HASHEMIYAN[*], P. PACKO[*], W.J. STASZEWSKI[*] AND T. UHL[*]

[*] AGH University of Science and Technology, Department of Robotics and Mechatronics,
Al. Mickiewicza 30, 30-059 Krakow, Poland,
email: zahra@agh.edu.pl, pawel.packo@agh.edu.pl,
w.j.staszewski@agh.edu.pl, tuhl@agh.edu.pl

Key Words: *Wave Propagation Modelling, Magnetic Resonance Elastography, Local Interaction Simulation Approach.*

Abstract. The Local Interaction Simulation Approach is proposed to study shear wave propagation modelling. These results indicate the capability of the method for shear wave propagation modeling in Magnetic Resonance Elastography investigations. The major advantage of the approach used is the reduction of computational effort.

1 INTRODUCTION

Mechanical properties of soft biological tissues are often used in medicine to diagnose cancer or tumor cells. Magnetic Resonance Elastography (MRE) [1-7] is a relatively new and emerging imaging technique based on this principle. This noninvasive method draws out differences in biomechanical properties of normal and abnormal tissues. Shear waves are generated in tissues by utilizing the application of stress or mechanical excitation. The resulting tissue motion is then analysed using phase contrast imaging that is achieved thanks to the Motion-Encoding Gradient (MEG) in a specific direction [1]. The MRE has been used for berets, brain and liver cancer diagnosis [7-10].

Analysis of tissue responses to applied stress (direct problem) and estimation of mechanical properties from measured responses (inverse problem) are formulated in elastography from well-established physical laws. Equations that relate biomechanical properties (i.e. shear modulus, Poisson's ratio, anisotropy, viscosity, nonlinearity and poroelasticity) to measured mechanical response are used.

It is well known that any reconstruction of shear modulus in complex media with heterogeneous boundary conditions is only practicable under certain assumptions and requires plane strain conditions that are challenging to fulfill [7]. Consequently, numerical simulations are used in MRE research studies in order to obtain a forward model that allows one capturing complex mechanical behavior of various soft tissues. The governing equations for various methods of elastography can be solved using Finite Element (FE) modelling [4,11]. FE models are used not only for the elasticity reconstruction algorithms [11,12] but also for the analysis of shear wave propagation in MRE gel phantoms [1,13-14]. For example a two-

dimensional (2-D) FE analysis was used in [14] to model agarose gel phantoms and examine material stiffness, density and boundary conditions of propagating shear waves. Then the shear wavelength from the simulated FE model was compared with the relevant result from MRE measurements and analytical models.

The aim of the present study is to build a computationally efficient three-dimensional gel phantom model for the analysis of shear wave propagation. In order to achieve this the Local Interaction Simulation Approach (LISA) [15,16] was applied. The LISA is a relatively new approach, which was recently used to investigate wave propagation in complex media with sharp impedance changes. Recent investigations in [17] demonstrate that the new implementation of LISA – based on a parallel algorithm and a Computer Unified Device Architecture (CUDA) that is available in low-cost graphical cards– offers computational superiority of the method over FE modeling. The work presented in this paper compares the LISA modeling results with FE results. Numerical simulations are validated using analytical solution in infinite elastic space and the MRE measurements - from a soft tissue mimicking agarose gel phantom.

2 THEORETICAL BACKGROUND

Elastic wave propagation in isotropic linear media is governed by the linear momentum balance equation given as

$$\sigma_{ij,i} + \rho b_i = \rho \ddot{u}_i \tag{1}$$

where $\sigma_{ij,i}$ is the divergence of stress tensor, ρ is the material density, b_i is an external volume force and $\ddot{u}_i$ represents the particle acceleration. The constitutive equation that relates the stress σ_{ij} to the strain ε_{ij} in a linear elastic solid can be given by

$$\begin{aligned} \sigma_{ij} &= \lambda \Delta \delta_{ij} + 2\mu \varepsilon_{ij} \\ \varepsilon_{ij} &= \frac{1}{2}(u_{ij} + u_{ji}) \end{aligned} \tag{2}$$

where δ_{ij} is the Kronecker delta, Δ represents the material dilatation given by $\Delta = \nabla . u = \varepsilon_{11} + \varepsilon_{22} + \varepsilon_{33}$, and λ, μ represent the Lame constants for the material and u_i represents particle displacement components. Combining equations (1) and (2) result in the equation of equilibrium

$$\nabla . \mu \nabla u + \nabla(\lambda + \mu) u = \rho \frac{\partial^2 u}{\partial t^2} \tag{3}$$

The solution to equation (3) with boundary conditions can be found only for simple canonical problems. For complex geometry and media the analytical solution cannot be established and numerical simulations are required.

2.1 Finite element model

FE modeling was used initially. This section briefly describes the model. The results were used for comparative analysis with LISA investigations. FE modelling of partial differential equations requires four steps. Firstly, mesh generation is performed, i.e. the geometry of the tissue is fragment to produce a mesh. Secondly, a weak form of the governing equation is derived using either the variational or weighted residual method [7]. Then, a basis or shape

function is introduced to the derived equation to generate a system of linear algebraic equations, which has the following form

$$[\,M\,]\{\ddot{u}\} + [k]\{u\} = \{P_e\} \tag{4}$$

where M and K are the mass and global stiffness matrices, respectively, P_e is the vector of dynamic forces and u is the vector of unknown displacements. Finally, external boundary conditions - associated with the problem - are imposed and the set of equations is solved.

The FE *Marc Mentat 2013* software package was used in the current study to simulate shear wave propagation in a MRE phantom. The phantom was modelled as a 3-D cylinder container filled with agarose gel. The dimensions of the container were: diameter - 200 mm and thickness - 20 mm.

The bottom of the cylindrical was fixed in the y direction in these numerical simulations. The cylinder was meshed using 2 × 2 × 8.5 mm elements in radial, axial and tangential directions respectively. The mesh was created using a symmetrical mesh system referable to radial, axial and tangential coordinates. Altogether 36 000 elements were used. The phantom was modeled as a homogenous isotropic elastic solid with the Poisson's ratio ν = 0.495. Sinusoidal harmonic motion was applied to the middle of the top surface to excite the phantom. The frequency of excitation was equal to 150 Hz. Three different values of Young's modulus were used - i.e. 30, 60 and 120 kPa – in order to investigate the relationship between the shear wavelength and the shear elastic modulus. Similarly, three different values of material density – i.e. $0.5\text{x}10^3$, $1\text{x}10^3$, and $2\text{x}10^3$ kg/m^3 - were studied. Material damping was assumed to be negligible. Transient dynamic analysis was applied in order to capture shear wave propagation. The time increment in this dynamic analysis was equal to 3.3×10^{-4} s. The shear wavelength λ_f in the FE model was obtained by estimating the distances between wave peaks directly from response waveforms. The same estimating approach was applied to the MRE experimental data.

2.2 Local interaction simulation approach for wave propagation

This section briefly describes the LISA model of shear wave propagation in the MRE phantom investigated. The geometry of the model and material properties used were the same as in the FE model described in the previous section.

The LISA can be used for wave propagation in any heterogeneous material of arbitrary shape and complexity. The method discretises the structure under investigation into a grid of cells and the material properties are assumed to be constant within each cell but may differ between cells. Discretisation in time is also used for wave propagation modelling. The algorithm can be proceed from the elastodynamic wave equation (5).

$$\nabla_\sigma(C\nabla_\varepsilon W) = \rho W_{,tt} \tag{5}$$

where C is the stiffness matrix, ∇_σ and ∇_ε are the differential operators matrices for stress and strain respectively, W is the vector of particle displacements, and ρ is the density. A comma before the subscript in equation (5) denotes differentiation. The C matrix contains stiffness components $C_{ij}^{(p)}$ that depend on Young's moduli, Poisson ratios and Kirchhoff's moduli for particular directions.

As illustrated in Figure 1, the structure is discretised into parallelepiped cells for the 3-D LISA wave propagation simulation. The junction of the eight cells characterizes the nodal point P. The second time derivatives across the eight cells are needed to converge towards a common value Ω at the point P. In Order to calculate a spatial derivative in the eight surrounding cells to P, The central difference scheme is utilized. Then to obtain the solution, stress continuity across adjacent cells is constrained.

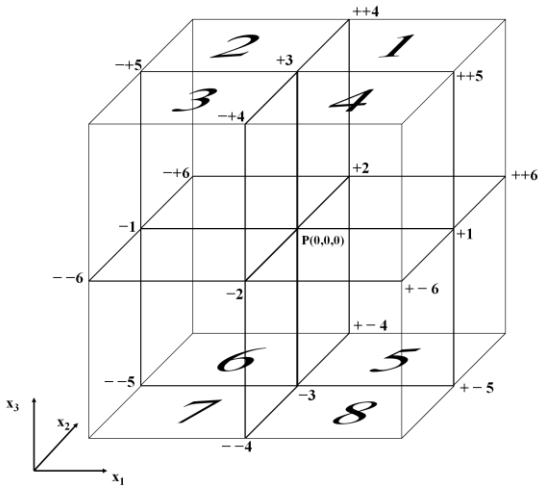

Figure 1: Eight elementary discretisation scheme used for wave propagation modeling in the LISA 3D.

The following iteration equations are acquired for each displacement component for a general orthotropic case,

$$\begin{aligned}\chi(u_{t+1}-2u_t+u_{t-1}) = -2u_0 \sum_{(i,k)}^{(1,11),(2,66),(3,55)} \frac{1}{\Delta x_i^2}\sum_{p=P} C_k^{(p)} \\ + \Delta x_2\left(w_0 \sum_{p}^{-\alpha(1)\alpha(3)P} C_{13+55}^{(P)} + 2\frac{1}{\Delta x_i}\sum_{p}^{P} u_{\alpha i} C_k^{(P)} + \sum_{r}^{1,3}\sum_{p}^{(r-2)\alpha(1)\alpha(3)P} w_{\alpha(r)r} C_{13-55}^{(P)} + \sum_{p}^{-P\alpha(1)\alpha(3)} w_{\alpha(1)\alpha(3)5} C_{13+55}^{(P)}\right) \\ + \Delta x_3\left(v_0 \sum_{p=SP} C_{12+66}^{(p)} + \sum_{r}^{1,2}\sum_{p}^{(-1)^r PS} v_{\alpha(r)r} C_{12-66}^{(P)} + \sum_{p}^{-PS} v_{\alpha(1)\alpha(2)6} C_{12+66}^{(P)}\right)\end{aligned} \tag{6}$$

$$\begin{aligned}\chi(v_{t+1}-2v_t+v_{t-1}) = -2v_0 \sum_{(i,k)}^{(1,66),(2,22),(3,44)} \frac{1}{\Delta x_i^2}\sum_{p=P} C_k^{(p)} \\ + \Delta x_1\left(w_0 \sum_{p}^{-\alpha(2)\alpha(3)P} C_{23+44}^{(P)} + 2\frac{1}{\Delta x_i}\sum_{p}^{P} v_{\alpha i} C_{(66,22,44)}^{(P)} + \sum_{r}^{2,3}\sum_{p}^{(2r-5)\alpha(2)\alpha(3)P} w_{\alpha(r)r} C_{23-44}^{(P)}\right. \\ \left. + \sum_{p}^{-P\alpha(2)\alpha(3)} w_{\alpha(2)\alpha(3)4} C_{23+44}^{(P)}\right) + \Delta x_3\left(u_0 \sum_{p=SP} C_{12+66}^{(p)} + \sum_{r}^{1,2}\sum_{p}^{(-1)^r PS} u_{\alpha(r)r} C_{12-66}^{(P)} + \sum_{p}^{-PS} u_{\alpha(1)\alpha(2)6} C_{12+66}^{(P)}\right)\end{aligned} \tag{7}$$

$$
\begin{aligned}
&\chi(w_{t+1} - 2w_t + w_{t-1}) \\
&\quad = -2w_0 \sum_{(i,k)}^{(1,55),(2,44),(3,33)} \frac{1}{\Delta x_i^2} \sum_{p=P} C_k^{(p)} \\
&\quad + \Delta x_1 \left(v_0 \sum_{p}^{-\alpha(2)\alpha(3)P} C_{23+44}^{(P)} + 2\frac{1}{\Delta x_i} \sum_{p}^{P} v_{\alpha i} C_{(55,44,33)}^{(P)} + \sum_{r}^{2,3} \sum_{p}^{(5-2r)\alpha(2)\alpha(3)P} w_{\alpha(r)r} C_{23-44}^{(P)} \right. \\
&\quad \left. + \sum_{p}^{P\alpha(2)\alpha(3)} w_{\alpha(2)\alpha(3)4} C_{23+44}^{(P)} \right) \\
&\quad + \Delta x_2 \left(u_0 \sum_{p=SP} C_{13+55}^{(p)} + \sum_{r}^{1,3} \sum_{p}^{(2-r)P\alpha(1)\alpha(3)} u_{\alpha(r)r} C_{13-55}^{(P)} + \sum_{p}^{-P\alpha(1)\alpha(3)} u_{\alpha(1)\alpha(3)5} C_{13+55}^{(P)} \right)
\end{aligned}
\tag{8}
$$

where Δx_i is grid spacing in i^{th} direction, Δt is the time step, $\alpha(i)$ denotes the i^{th} column of the α matrix of signs, displacement components are taken at time t and point (0,0,0) if not stated otherwise. The p index in the summation formula conveys the sign of the summed component.

The local interaction nature of boundaries in the model is one of the major advantages of the LISA algorithm when used for wave propagation. The Sharp Interface Model (SIM) [17] is utilized to average physical properties at interface grid points, which deputize intersections of eight elementary cells. It means that cells are treated as discontinuous also; displacements and stresses are matched at interface grid points. The SIM permits for a more physical and unambiguous treatment of interface discontinuities for different layers of material than typical FD schemes. Typically FD is not very accurate for sharp interfaces of high impedance mismatch due to require parameter smoothing across material interfaces, which depends on the applied scheme. When wave propagation problems in complex media with complex boundaries are studied, the SIM conduce to more accurate results. More details relevant to 3-D wave propagation implementation can be found in [16]. The algorithm has been used successfully for Lamb wave propagation investigations for damage detection [17]

3 RESULTS

This section presents numerical results from the FE- and LISA-based numerical simulations of shear wave propagation. The simulated results are compared with the experimental MRE results reported in [14].

The radial shear wave propagation images for the FE and LISA models are shown in Figure 2. The values of Young's modulus and density used in these simulations are equal to E = 90 kPa and $\rho = 1.0 \times 10^3$ kg/m^3, respectively. Both wave propagation patterns reveal the same wavelengths. Small differences in theses images can be attributed to different formulations of the FE and LISA models and significant numerical damping of the LISA method for the assumed material properties and mesh.

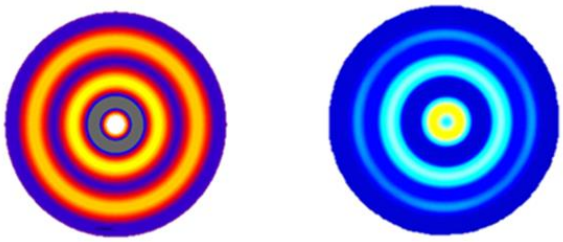

Figure 2: LISA (left) and FE (right) wave propagation images from the cylindrical model of the MRE phantom.

Subsequently, out of plane displacement components in the radial direction of the phantom's models were acquired. The simulated results are compared with the experimental MRE results in Figure 3. These results were produced for the Young's modulus and density equal to E = 90 kPa and $\rho = 1.0 \times 10^{3}$ kg/m^3, respectively. Here, the shear wavelengths can be estimated from the distance between the two successive peaks (or valleys). The values of shear wavelength were estimated as 39 and 36 mm for the FE and LISA models, respectively. This compares relatively well with the 38.00±2.12 mm value obtained from the MRE experimental test. The simulated results and experimental data are in relatively good agreement, although some minor discrepancies can be observed.

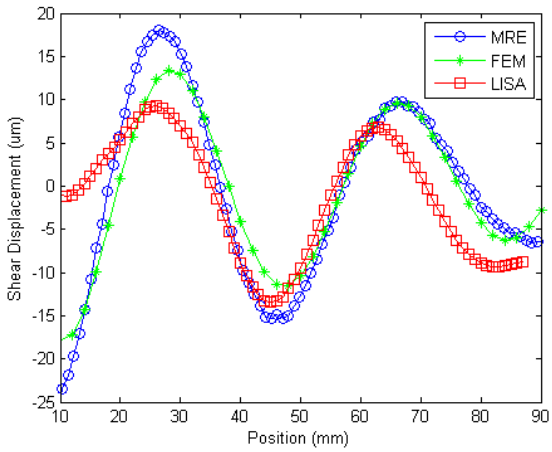

Figure 3: Comparison of the simulated FE and LISA displacement waveforms the relevant MRE measurement for the cylindrical agar gel phantom.

Next, the dependency of simulated shear wavelengths on different elastic moduli was further analysed and compared with the analytical approximate solution. For isotropic elastic solids (assumed to be infinite) the local shear modulus can be estimated from [1]

$$\lambda = \frac{1}{f}\sqrt{\frac{G}{\rho}} \qquad G = \frac{E}{2(1+\nu)} \tag{9}$$

Figure 4 presents the simulated shear wavelengths with different elastic moduli E assigned to 30, 60 and 90 kPa and material densities ρ assigned to 0.5, 1 and 2×10^{3} kg/m^3. Here, the solid curves represent the shear wavelength obtained from equation (9).

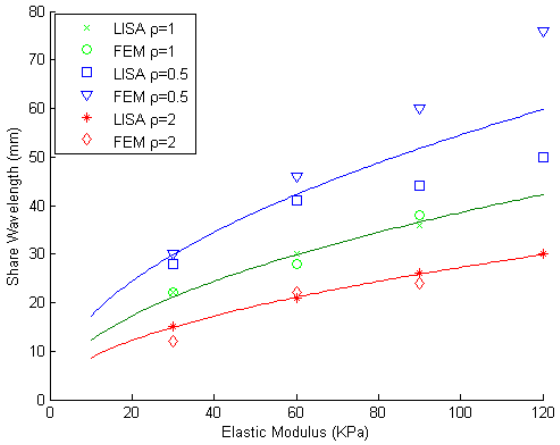

Figure 4: Simulated shear wavelengths for different elastic modules and material densities. Analytical solutions are given by solid lines

The results in Figure 4 show good agreement between numerical and analytical solutions for small values of elastic moduli. This is particularly relevant for the LISA model. It is also important to note that numerical simulations based on the LISA model re computationally much less expensive than the same simulations based on the FE model. The former required only 10 s whereas the latter involved 2 640 s of computation time. A significant discrepancy between numerical (both models) and analytical results has been observed only or higher values of elastic moduli corresponding to larger wavelengths.

4 CONCLUSION

Proper understanding of shear wave propagation behaviour in soft tissues is important in MRE tests. A simple 3-D FE and LISA models were built to examine several factors that influence shear modulus estimation in homogenous phantoms, with the shear wavelength being the primary parameter in characterizing shear modulus.

The results presented show good agreement between numerical/analytical models and experimental MRE measurements. The estimated shear wavelengths from the FE and LISA models are reasonably close to the theoretical values for homogenous elastic cylindrical phantoms and short wavelengths investigated. The LISA model presented in the paper is particularly attractive due to significant reductions of computational effort.

ACKNOWLEDGEMENTS:

The work presented in this paper was supported by the Foundation for Polish Science under the research WELCOME project no. 2010-3/2 (Innovative Economy, National Cohesion Programme, and EU). The authors are grateful to Dr Q. Chen and Prof. K.N. An from the Biomechanics Research Laboratory at Mayo Clinic Rochester for the MRE experimental data.

REFERENCES

[1] Muthupillai, R. Lomas, D.J. Rossman, P.J. Greenlea, J.F. Manduca, A. and Ehman, R.L. Magnetic-resonance elastography by direct visualization of propagating acoustic strain waves Science. (1995)5232:1854–7.

[2] Manduca, A. Oliphant, T.E. Dresner, M.A. Mahowald, J.L. Kruse, S.A. Amromin, E. Felmlee, J.P, Greenleaf, J.F. and Ehman, R.L .Magnetic resonance elastography: non-invasive mapping of tissue elasticity Med. Image.Anal. (2001) 5:237–54.

[3] Bishop, J. Samani, A. Sciarretta, J. and Plewes, D. Two-dimensional MR elastography with linear inversion reconstruction: methodology and noise analysis, Phys. Med. Biol. (2000) 45:2081–91.

[4] Weaver, J.B. VanHouten, E.E. Miga, M.I. Kennedy, F.E. and Paulsen, K.D. Magnetic resonance elastography using 3D gradient echo measurements of steady-state motion. Med.Phys. (2001) 28:1620–8.

[5] Mariappan, Y.K. Glaser, K.J. and Ehman, R. Magnetic Resonance Elastography: a Review. Clin Anat. (2010)23:497–511.

[6] Parker, K.J. Doyley, M.M and Rubens, D.J. Imaging the elastic properties of tissue: the 20 year perspective. Phys.Med. Biol. (2011)56:R1–29.

[7] Doyley, M.M. Model-based elastography: a survey of approaches to the inverse elasticity problema. Phys. Med. Biol. (2012) 57: R35–R73.

[8] Talwalkar, J.A. Yin, M. Fidler, J.L. Sanderson, S.O. Kamath, P.S. and Ehman, R.L. Magnetic resonance imaging of hepatic fibrosis: emerging clinical applications. Hepatology. (2008) 47:332–342.

[9] McKnight, A.L. Kugel, J.L. Rossman, P.J. Manduca, A. Hartmann, L.C. and Ehman, R.L. MR elastography of breast cancer: preliminary results. American Journal of Roentgenology. (2002) 178:1411–1417.

[10] Sinkus, R. Lorenzen, J. Schrader, D. Lorenzen, M. and Dargatzmand, D. High-resolution tensor MR elastography for breast tumour detection.Phys. Med. Biol. (2000)45:1649–64.

[11] Vanhouten, E.E. Miga, M.I. Weaver, J.B. Kennedy, F.E, and Paulsen K.D. Three-dimensional subzone-based reconstruction algorithm for MR elastography Magn. Reson. Med. (2001)45: 827–37.

[12] Brigham, J.C. Aquino, W. Mitri, F.G. Greenleaf, J. and Fatemi, M. Inverse estimation of viscoelastic material properties for solids immersed in fluids using vibroacoustic techniques.J. Appl. Phys. (2007) 101: 023509-14.

[13] Ringleb, S.I. Chen, Q. Manduca, A. Ehman, R.L. and An, K.N. Quantitative shear wave magnetic resonance elastography: comparison to a dynamic shear material test. Magn Reson Med. (2005) 53: 1197-1201.

[14] Chen, Q. Ringleb, S.I. Manduca, A. Ehman, R.L. and An, K.N. A finite element model for analyzing shear wave propagation observed in magnetic resonance elastography. Journal of Biomechanics. (2005) 38:2198–2203.

[15] Delsanto, P. Whitcombe, T. HChaskelis, H. and Mignogna, R. Connection Machine Simulation of Ultrasonic Wave Propagation in Materials. II: The Two-Dimensional Case, Wave Motion, (1994)20: 295- 314.

[16] Delsanto, P. Schechte, R.S. and Mignogna, R.S. Connection Machine Simulation of Ultrasonic Wave Propagation in Materials. III: The Three-Dimensional Case. Wave Motion. (1994)26:329–339.

[17] Packo, P. Bielak, T. Spencer B. Staszewski, W.J. and Uhl, T. Lamb wave propagation modelling and simulation using parallel processing architecture and graphical cards Smart Mater. Struct. (2012)21:1-13.